Phage Selection of Cyclic Peptides Inhibiting Aminoglycoside Phosphotransferases to Control Resistant Bacteria

Qiannan Guo, Hui Zeng, and Xu-Dong Kong*

ACCESS | Metrics & More | Article Recommendations | SI Supporting Information

ABSTRACT: The clinical threat of aminoglycoside phospho-transferases (APHs) stems from their efficient inactivation of aminoglycosides, driving multidrug resistance through broad-spectrum antibiotic modification. While peptide-based inhibitors represent a promising therapeutic modality, current candidates lack sufficient potency against APHs. To address this limitation, we employed phage display technology to screen large cyclic peptide libraries (structural diversity $>10^{11}$) against APH(3′)-Ia, a clinically relevant enzyme derived from *Escherichia coli*. Our selection identified cyclic peptide families exhibiting nanomolar binding affinities characterized by two conserved motifs: CXW(P/L)LC and CP(W/F)YC. Intriguingly, divalent cations (Mg^{2+} and Ca^{2+}) enhanced peptide−APH interactions, suggesting a metal-depend-ent binding mechanism. Competitive fluorescence polarization assays revealed that these cyclic peptides primarily occupy the ATP-binding pocket of APH(3′)-Ia, with representative candidate A-L3 demonstrating significant enzymatic inhibition. This study establishes a foundation for developing APH-targeted antibiotic adjuvants through (1) identification of novel cyclic peptide scaffolds with inhibitory potential, (2) elucidation of divalent metal ion effects on inhibitor binding, and (3) mechanistic insights into ATP-binding site competition. These findings provide critical structural and functional information to guide the rational design of next-generation antibiotic resistance breakers.

Phage selection of cyclic peptide for APH — Binding site analysis. $K_d = 63 \pm 6$ nM
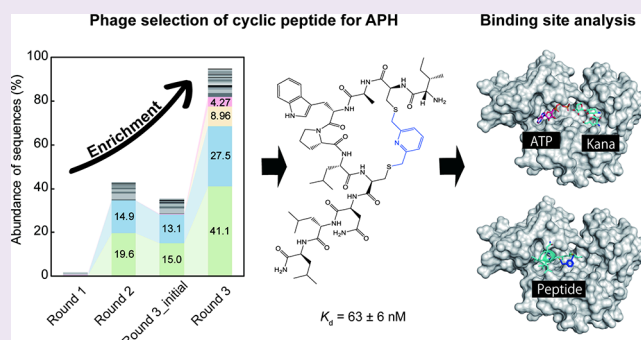
INTRODUCTION

Antibiotic resistance has emerged as one of the most pressing public health challenges worldwide.[1] The increasing prevalence of resistant bacterial strains not only threatens the effectiveness of current treatments but also imposes a significant burden on healthcare systems. At the molecular level, antibiotic resistance often arises from bacterial mechanisms that inactivate or evade the effects of drugs.[2] One promising strategy to overcome this problem is the use of enzyme inhibitors as adjuvants, which can restore the antibacterial activity of existing antibiotics.[3,4] This approach has already found success in the β-lactam field, where inhibitors are coadministered with antibiotics to neutralize β-lactamases.[5]

Among the various classes of antibiotics, aminoglycoside antibiotics (AGAs) play a vital role in treating infections, particularly those caused by Gram-negative pathogens.[6] AGAs exert their effect by binding directly to rRNA and inducing mistranslation during protein synthesis.[6−8] However, bacteria have evolved resistance mechanisms to counter these effects. A key resistance mechanism is the enzymatic modification of AGAs by aminoglycoside modifying enzymes (AMEs), which inactivate the antibiotic through specific chemical modifica-tions.[2] AMEs are generally classified into three families: aminoglycoside phosphotransferases (APHs), aminoglycoside acetyltransferases (AACs), and aminoglycoside nucleotidyl-

transferases (ANTs). For example, APH(3′)-Ia, which phosphorylates the 3′-hydroxyl group of many AGAs, is highly efficient and contributes significantly to resistance in clinical isolates.[9,10] The coding gene of APH(3′)-Ia was originally found on the transposon Tn903 from *E. coli*,[11] which have been identified among clinical isolates.[12,13] APH(3′)-Ia has high catalytic activity against a broad spectrum of AGAs, including lividomycin, neomycin, paromomycin, ribostamycin, and kanamycin.[6,14]

Over recent decades, cyclic peptides have gained prom-inence in drug development due to their excellent affinity, stability, and specificity.[15,16] Phage display, a high-throughput *in vitro* screening technique, has been instrumental in selecting both linear and cyclic peptides as specific ligands for target proteins.[17−20] This technology has enabled the discovery of numerous drug candidates, including clinically approved molecules such as adalimumab and ecallantide,[19,21] as well as
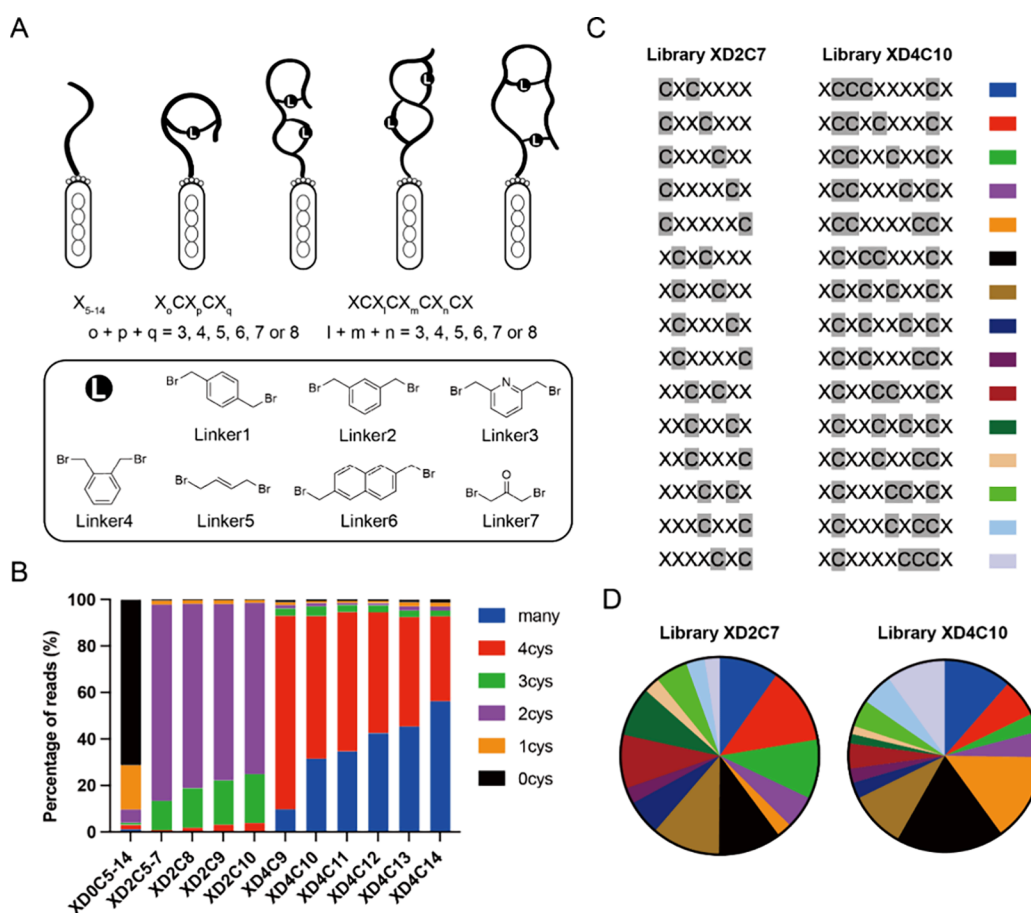
Figure 1. Design and quality characterization of phage-displayed cyclic peptide libraries. (A) Library design. The letter "L" represents chemical linkers that cross-link pairs of cysteines in the phage-displayed peptides. Peptides with two or four cysteines undergo cyclization via these linkers to form monocyclic or double-bridged cyclic peptides. (B) Cysteine distribution across the 11 sublibraries. The sublibrary names are formatted as "XD[number]C[number]", where the first number represents the number of cysteines in the peptide, and the second number indicates the peptide length. (C) Peptide formats in sublibraries XD2C7 and XD4C10. The letter "X" represents random amino acid, while "C" designates the cysteine. (D) Proportions of peptide formats in XD2C7 and XD4C10 libraries. The distribution is based on the next-generation sequencing results.

promising candidates like BT-1718—a bicyclic peptide currently undergoing phase I/IIa clinical trials.[22] Despite these advances, there is a notable scarcity of effective cyclic peptides that target antibiotic resistance proteins.[4]

In light of this, recent innovations in peptide cyclization strategies and peptide scaffold design have dramatically increased the structural diversity of phage-displayed cyclic peptide libraries. Cyclization reagents containing three thiol-reactive groups, such as 1,3,5-tris(bromomethyl)benzene (TBMB),[20] 1,3,5-triacryloyl-1,3,5-triazinane (TATA), and N,N',N''-(benzene-1,3,5-triyl)tris(2-bromoacetamide) (TBAB)[23] have been effectively used to generate bicyclic peptides by cyclizing linear phage-encoded peptides containing three cysteine residues (i.e., CX_6CX_6C, XCX_3CX_3CX, and XCX_4CX_4CX).[20,24] More recently, metal ions such as bismuth-(III) and arsenic(III) have also been employed to produce bicyclic peptides from three cysteine peptides.[25,26] For the construction of diverse monocyclic or double-bridged peptides, bis-electrophilic reagents have also been successfully applied to modify the peptides that displayed three or four cysteines with varied scaffolds and lengths (i.e., XCX_3CX_3CX and XCX_4CX_4CX, or $XCX_mCX_nCX_oCX$, $m + n + o = 3-8$).[27,28] Furthermore, the genetically encoded cysteine-reactive noncanonical amino acid O-(2-bromoethyl)-tyrosine (O2beY) has been incorporated into displayed peptides as an internal

cyclization handle to generate macrocyclic peptides.[29] Continued progress in linker chemistry and scaffold design has significantly expanded both the diversity and sequence space of phage-displayed peptide libraries.[16,30,31] These advancements suggest that cyclic peptides could serve as potent inhibitors of AMEs, such as APH(3′)-Ia, thereby offering a new approach to overcoming AGA resistance. Previous studies have demonstrated that small-molecule inhibitors—including pyrazolopyrimidine derivatives and bisubstrate analogues—can attenuate APH(3′)-Ia activity and restore AGA efficacy.[32,33] However, peptide-based inhibitors, despite their potential, remain largely unexplored in this context.

In the present study, we address this gap by focusing on the discovery of high-affinity cyclic peptides that specifically target APH(3′)-Ia (hereafter referred to as APH). Utilizing an ultrahigh-diversity phage display library (with a diversity of 10^{11}), we conducted three rounds of in vitro selection and successfully identified several candidate cyclic peptides. These peptides exhibit low micromolar to nanomolar binding affinities and demonstrable inhibitory effects on APH activity. Our findings not only provide novel candidates for the development of adjuvant therapies to restore AGA activity but also establish a new chemical scaffold for further optimization in combating antibiotic resistance.

■ RESULTS AND DISCUSSION

Construction and Diversity Analysis of Phage-Displayed Cyclic Peptide Libraries. The structural diversity of a peptide library is a critical factor in the success of phage selection. To achieve high diversity, we designed phage display peptide libraries containing zero-, two-, or four-cysteine residues. These libraries were further modified using seven chemical linkers, enabling the generation of peptides in three distinct configurations: linear peptides, monocyclic peptides, and double-bridged peptides (Figure 1A).

For library construction, plasmids containing peptide-encoding DNA fragments were generated through the self-ligation of whole-plasmid PCR products, followed by electroporation into *E. coli* TG1 cells. A total of 11 sublibraries were constructed, each categorized by cysteine composition: XD0C5−14 featuring linear peptides without fixed cysteine residues; XD2C5−7, XD2C8, XD2C9, and XD2C10 containing peptides with two fixed cysteines; and XD4C9, XD4C10, XD4C11, XD4C12, XD4C13, and XD4C14 incorporating peptides with four fixed cysteines.

To evaluate the library quality, we analyzed the diversity of phage-displayed peptides using next-generation sequencing (NGS). The results showed that ∼70% of sequences in library XD0C5−14 encoded peptides without cysteine residues. Likewise, over 75% of sequences in libraries XD2C5−XD2C10 contained peptides with two cysteines, while approximately 90% of sequences in libraries XD4C9−XD4C14 encoded peptides with at least four cysteines (Figure 1B). These findings aligned with the expected amino acid distributions, confirming the successful construction and high quality of the phage-displayed peptide libraries.

Peptides in library XD0C5−14 were designed in the form of X_{5-14}, consisting of 5−14 random amino acids without fixed cysteines (Figure S1). In sublibraries XD2C5−XD2C10, peptides followed the format $X_oCX_pCX_q$ (where $o + p + q =$ 3, 4, 5, 6, 7, or 8, $p > 0$), featuring two cysteines flanked and spaced by variable numbers of random amino acids. This design created diverse backbone scaffolds, as exemplified by library XD2C7 (Figure 1C). In total, the $X_oCX_pCX_q$ format generated 116 unique cysteine-spacing patterns (Figure 1C and Figure S1) and the sublibraries of XD2C5−XD2C10 were constructed with approximately 2×10^9 distinct peptide sequences (Table S1). Further cyclization with seven chemical linkers expanded the diversity to nearly 1.4×10^{10} single-bridged peptides.

In sublibraries XD4C9−XD4C14, peptides were designed in the form $XCX_lCX_mCX_nCX$ (where $l + m + n =$ 3, 4, 5, 6, 7, or 8), featuring four cysteines spaced by varying numbers of random amino acids and flanked by one additional random residue at both ends. This design produced diverse backbone scaffolds, exemplified by library XD4C10 (Figure 1C). In total, the $XCX_lCX_mCX_nCX$ format generated 155 unique cysteine-spacing patterns (Figure 1C and Figure S1) and the sublibraries of XD4C9−XD4C14 were constructed with approximately 5.4×10^9 distinct peptide sequences. Further modification with chemical linkers enabled three possible cysteine-pairing modes per peptide, expanding the diversity to as many as 1.1×10^{11} double-bridged peptides using seven cyclization linkers (Figure 1A). NGS analysis of libraries XD2C7 and XD4C10 showed that the proportions of each peptide format ranged from 2.4 to 12.6% and from 1.4 to 18%, respectively (Figure 1D and Figure S2). Taken together, these

data indicate that large phage display libraries with a high diversity (10^{11}) were successfully generated.

Enrichment of Cyclic Peptides Binding to APH. To select cyclic peptides that inhibit APH activity, we immobilized biotinylated APH (Figure S3) on magnetic beads and used them to pull out cyclic peptide binders displayed on the phage. Specifically, the 11 sublibraries were cultured overnight to amplify phage displaying cysteine-rich peptides. The cysteines in the peptides were cyclized with chemical linkers 1−7 (Figure 1A) following reduction with tris(2-carboxyethyl)-phosphine (TCEP). These chemical linkers that containing two thiol-reactive groups have been reported to efficiently cyclize the peptides containing four cysteine moieties under phage-selection conditions.[27] As a control, an aliquot of the phage library was treated with TCEP but without cyclization. The eight samples were panned separately against biotinylated APH immobilized on magnetic streptavidin beads (round 1 and round 3) or neutravidin beads (round 2) to avoid enriching streptavidin binders. To select for cyclic peptides with higher affinities, the stringency of selection was increased by reducing the target protein dose, using 0.5, 0.25, and 0.05 μg for each linker in rounds 1, 2, and 3, respectively.

The titer of the phage captured by the target on beads was monitored throughout the three rounds of selection. For the first round, 1.3×10^{14} of phages were purified from 11 cultures of 250 mL each, and 1.2×10^{12} to 4.4×10^{12} infective phages, after being modified with different linkers, were used for panning. From this, 7.0×10^5 to 2.8×10^6 of them were captured and used to infect *E. coli* TG1 cells for the amplification of phage (Figure 2A). The preparation of phage for the second and third round of selection was
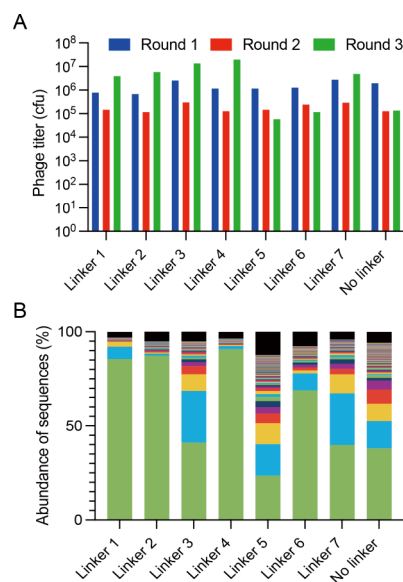

Figure 2. Phage titer and sequence enrichment across the selection. Three rounds of phage selection were performed against APH, followed by measurement of the selected phage titer and next-generation sequencing of the enriched peptide library. Seven chemical linkers along with a control condition without a linker were used to generate cyclic peptide libraries for selection. (A) Phage titer analysis over three rounds of selection under eight different conditions. (B) Distribution of the abundance for the 200 most frequent peptide sequences from round 3, as determined by NGS. The fraction of peptide sequences less abundant than the top 200 is shown at the top of the stacked bar chart, highlighted in black.
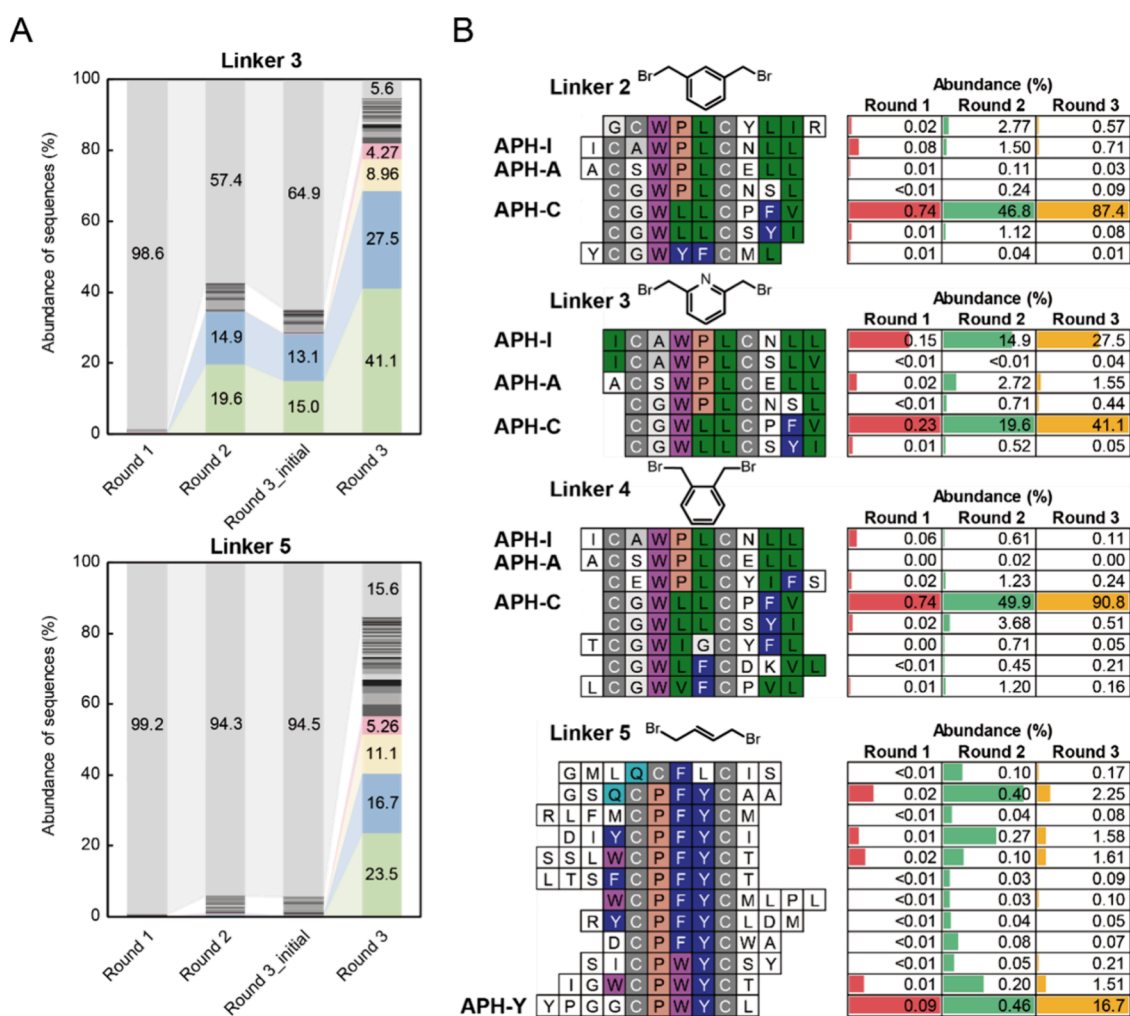
Figure 3. Enrichment and consensus analysis of cyclic peptide sequences. (A) Abundance of peptide sequences enriched across rounds 1 to 3 using linker 3 and linker 5. "Round 3_initial" represents the sequencing data of the phage library sample prior to the panning step of round 3. Numbers indicate the proportion of each peptide sequence or fraction. Sequences less abundant than the top 200 are grouped at the top of the stacked bar chart and are shown in gray. (B) Highly enriched peptides identified from phage libraries after three rounds of selection using linkers 2, 3, 4, or 5. Peptides with similar sequences are grouped and aligned with conserved regions highlighted in color. The relative abundance of each peptide is shown, and colored frames represent changes in abundance across selection rounds based on NGS results.

performed in a 25 mL culture for each condition, yielding an average of 1.5×10^{11} and 4.4×10^{11} infective phages after modification with linkers. The titer of captured phage increased significantly from round 2 to round 3, especially for linkers 2, 3, 4, and 7. After three rounds of selection, the capture yields (eluted phage/loaded phage) increased from 1.2×10^{-6} to 6.3×10^{-5} for linker 4 cyclized conditions, indicating successful enrichment of target-binding peptides (Figure 2A).

Subsequently, the peptide-encoding DNA sequences of the selected phage samples from each round as well as the phage samples prior to the panning step of round 3 were amplified by PCR using primers with unique barcode sequences (Table S2) and sequenced on the Illumina novaseq platform. MATLAB scripts were used to separate the sequences of different samples based on their barcodes, translate the nucleotide sequences into amino acid sequences, and cluster the peptide sequences into different consensus groups.[34] NGS results of round 3 showed that the abundance of the dominant selected peptide under different linker conditions ranged from 23.5 to 90.8%, indicating successful enrichment of target-binding peptides (Figure 2B).

By analyzing the proportion of peptide sequences in the NGS data from phage samples, we were able to track the enrichment of each sequence across the selection process. In addition, based on the prior panning sample of round 3, the changes in peptide proportions during both amplification and panning with the target could be distinguished. Specifically, the data for linkers 3 and 5 were analyzed in more detail, showing that peptides started to be significantly enriched in round 2 for linker 3 and round 3 for linker 5, respectively. As shown in Figure 3A, the relative abundances of selected peptides APH-I and APH-C increased from 0.15 and 0.23% (round 1) to 14.9 and 19.6% (round 2), reaching 27.5 and 41.1% (round 3) under linker 3 conditions. In contrast, the relative abundance of selected peptide APH-Y increased from 0.09% (round 1) to 0.46% (round 2) and then to 16.7% (round 3) under linker 5 conditions (Figure 3A). Additionally, the distribution of peptides in the phage sample from round 3-initial resembled that of round 2, indicating that no significant bias occurred during the amplification of the phage (Figure 3A).

Similar consensus groups were observed in two-cysteine peptides across most linker conditions (Figure 3B). The

consensus groups of APH-I, APH-A, and APH-C were the most abundant under linkers 2−4 and the second most abundant under linker 7. These groups contained the conserved motif "CXW(P/L)LC". In contrast, the consensus group of APH-Y, which harbored the conserved motif "CP(W/F)YC" under linker 5 conditions, was significantly different. This group was relatively less abundant compared to peptides containing "CXW(P/L)LC" in other linkers, and it became enriched only by round 3 (Figure 3A). Interestingly, no four-cysteine peptides were significantly enriched in our selection against APH, and we speculate that this may be due to two factors. First, the binding pocket of APH may better accommodate monocyclic peptides than bicyclic structures. Second, monocyclic peptides benefit from higher avidity effects, as they are displayed on phages at pentavalent levels. In contrast, each isomer of a bicyclic peptide derived from a four-cysteine sequence is likely displayed at only monovalent or bivalent levels.

Affinity of Cyclic Peptides to Target Protein. To determine the binding affinities of the enriched peptides to APH, four peptides (APH-C, APH-I, APH-A, and APH-Y) were synthesized with a C-terminal fluorescein moiety and cyclized with the corresponding linkers (Table S3). The affinity of these peptides was then tested by fluorescence polarization. For the peptide APH-A, four cyclic counterparts (A-L2, A-L3, A-L4, and A-L7) were generated by cyclization using linkers 2, 3, 4, and 7, respectively (Figure S4). A-L2, A-L3, and A-L4 exhibited submicromolar affinities, with K_d of 0.26 ± 0.02, 0.27 ± 0.03, and 0.36 ± 0.03 μM, respectively, while A-L7 showed more than a 10-fold weaker affinity ($K_d = 3.68 \pm 0.49$ μM, Figure 4A and Figure S5).

Similarly, three purified cyclic counterparts of peptide APH-C exhibited affinities of 0.96 ± 0.08, 0.75 ± 0.07, and 0.58 ± 0.06 μM for C-L2, C-L3, and C-L4, respectively (Figure 4B and Figure S5). The four purified cyclic peptides of APH-I (I-L2, I-L3, I-L4, and I-L7) displayed significantly better affinities with K_d of 0.10 ± 0.01 μM, 63 ± 6 nM, 0.14 ± 0.01 μM, and 0.80 ± 0.06 μM, respectively (Figure 4C and Figure S5). For the APH-Y enriched under linker 5 conditions, the K_d of its cyclic counterpart Y-L5 against APH is 0.40 ± 0.05 μM (Figure 4D and Figure S5). The linear and oxidized forms of representative peptides APH-C, APH-I, and APH-Y showed no affinity to APH (Figure S5). In summary, a series of candidate cyclic peptides, derived from sequences APH-C, APH-I, APH-A, and APH-Y, have been effectively identified from the three rounds of phage selection.

Previous efforts to develop APH inhibitors have focused primarily on small molecules. For example, derivatives of pyrazolopyrimidine targeting eukaryotic protein kinases (ePKs) were shown to inhibit APH with K_i values in the 3.8−93 μM range,[32] and bisubstrate analogues achieved the best K_i values of approximately 3.0 μM.[33] However, although peptide-based inhibitors (both cyclic and linear) have been reported, they do not show superior affinity, with IC_{50} or K_i values in the 5.0−79 μM range.[35] Interestingly, the cyclic peptides identified here (especially I-L3, $K_d = 63$ nM) show binding affinities to APH that exceed those of previously reported small molecules and peptides. This demonstrates that phage selection can produce high-affinity APH ligands suitable for further development.

Effect of Divalent Metal Ions on the Affinities of Cyclic Peptides. During the affinity characterization of cyclic peptides, binding measurements were initially conducted in
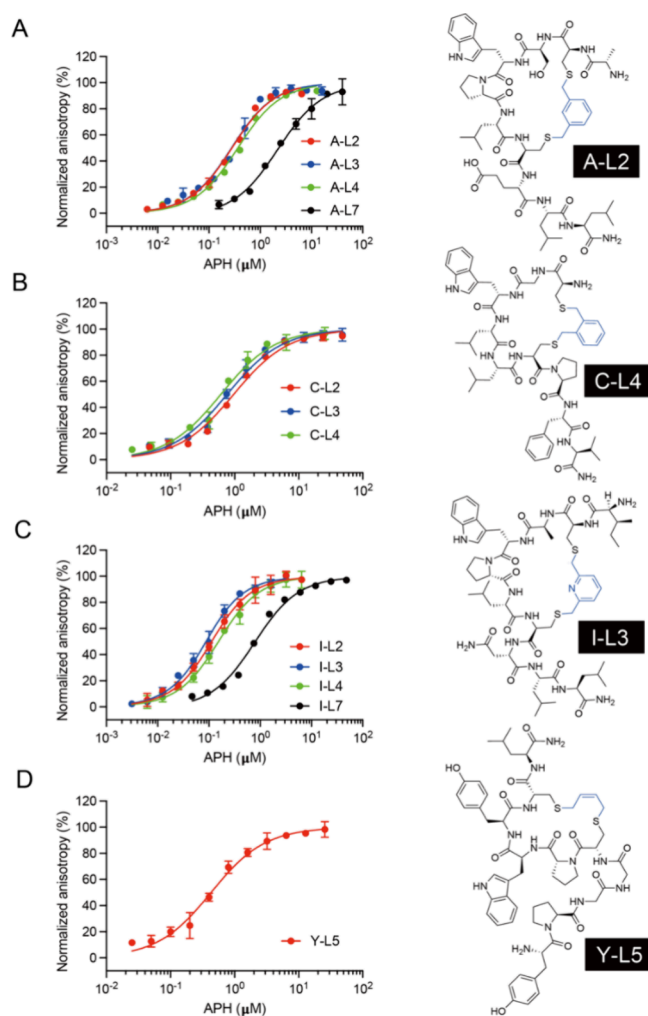

Figure 4. Affinity assays of cyclic peptides. Cyclic peptides derived from APH-A (A), APH-C (B), APH-I (C), and APH-Y (D), each modified with different chemical linkers, were tested for binding to APH. The binding affinity of the candidate cyclic peptides was measured using fluorescence polarization. The structures of four candidate cyclic peptides, A-L2, C-L4, I-L3, and Y-L5, are shown. Mean values and standard deviations from three independent measurements are presented.

two buffer systems: (1) standard PBS buffer (137 mM NaCl, 1 mM KCl, 4 mM Na_2HPO_4, 0.7 mM KH_2PO_4, pH 7.4, and 0.01% Tween 20) and (2) the reaction buffer (50 mM Tris−Cl pH 7.5, 40 mM KCl, 10 mM $MgCl_2$, and 0.01% Tween 20). Notably, significant differences in binding affinities were observed between these conditions. Considering the use of buffer W2 (10 mM Tris−Cl pH 7.4, 150 mM NaCl, 10 mM $MgCl_2$, 1 mM $CaCl_2$, 1% (w/v) BSA, and 0.1% (v/v) Tween 20) as incubation buffer in phage selection, we supposed that divalent metal ions might play a potential regulatory role in the interaction between cyclic peptides and APH. To investigate this hypothesis, the dissociation constants (K_d) of four candidate cyclic peptides were systematically evaluated in two additional buffer conditions: 50 mM Tris (pH 7.5), 40 mM KCl, with the addition of (i) 1 mM Ca^{2+} or (ii) no divalent metal ions (Figure 5).

For three cyclic peptides with the CXW(P/L)LC motif, the presence of 10 mM Mg^{2+} significantly enhanced binding affinity, with K_d values improved by 2.7- to 6.7-fold compared
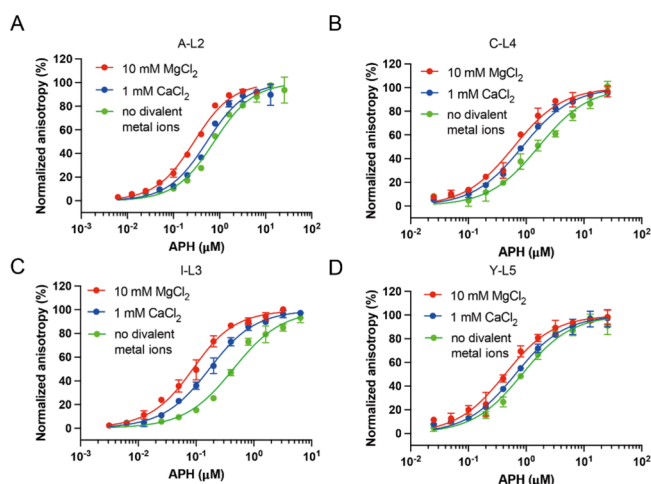
Figure 5. Influence of metal ions on the binding of cyclic peptides to APH. Binding affinities were determined using fluorescence polarization under three conditions, in a buffer containing 50 mM Tris (pH 7.5), 40 mM KCl, with the addition of 10 mM MgCl₂, 1 mM CaCl₂, or in the absence of divalent metal ions. Results are shown for four candidate cyclic peptides: A-L2 (A), C-L4 (B), I-L3 (C), and Y-L5 (D). Data represent the mean ± standard deviation (SD) from three independent measurements.

observed with 1 mM Ca^{2+} (0.51 ± 0.06 μM for A-L2, 0.83 ± 0.05 μM for C-L4, and 0.14 ± 0.01 μM for I-L3), indicating a weaker facilitating effect compared to that of 10 mM Mg^{2+} (Figure 5A−C). In contrast, the fourth peptide (Y-L5) exhibited less pronounced metal ion dependence. Its K_d values in Mg^{2+}-, Ca^{2+}-, and divalent metal-free buffers were 0.40 ± 0.05, 0.62 ± 0.05, and 0.81 ± 0.09 μM, respectively (Figure 5D), suggesting that the regulatory role of metal ions may be motif-specific. Collectively, these results demonstrate that both Mg^{2+} and Ca^{2+} enhance the binding affinity of cyclic peptides to APH, with Mg^{2+} (10 mM) exerting a more pronounced effect than Ca^{2+} (1 mM). This observation implies that metal ions likely stabilize specific conformational and electrostatic interactions during peptide−APH complex formation.

Divalent metal ions such as Mg^{2+} and Ca^{2+} are well known to modulate enzyme−substrate interactions and catalytic activity. In the previously published ternary complex of kanamycin A, ATP, and APH, two Mg^{2+} ions coordinate directly with the ATP phosphate backbone.[33,36] Likewise, the crystal structure of the APH·Ca^{2+}·ATP complex (PDB ID: 4EJ7) shows two Ca^{2+} ions simultaneously bridged to the ATP phosphates, specific enzyme residues, and ordered water molecules.[32] Together with our binding data—where peptide affinity increases markedly in the presence of 10 mM Mg^{2+} or 1 mM Ca^{2+} compared to metal-free buffer (Figure 5)—this suggests that these divalent cations may coordinate peptide− enzyme interactions at the interface, requiring validation by structural studies. Accordingly, including physiologically relevant concentrations of Mg^{2+} or Ca^{2+} in the phage-selection buffer should better recapitulate the native active site environment and thereby accelerate the identification of
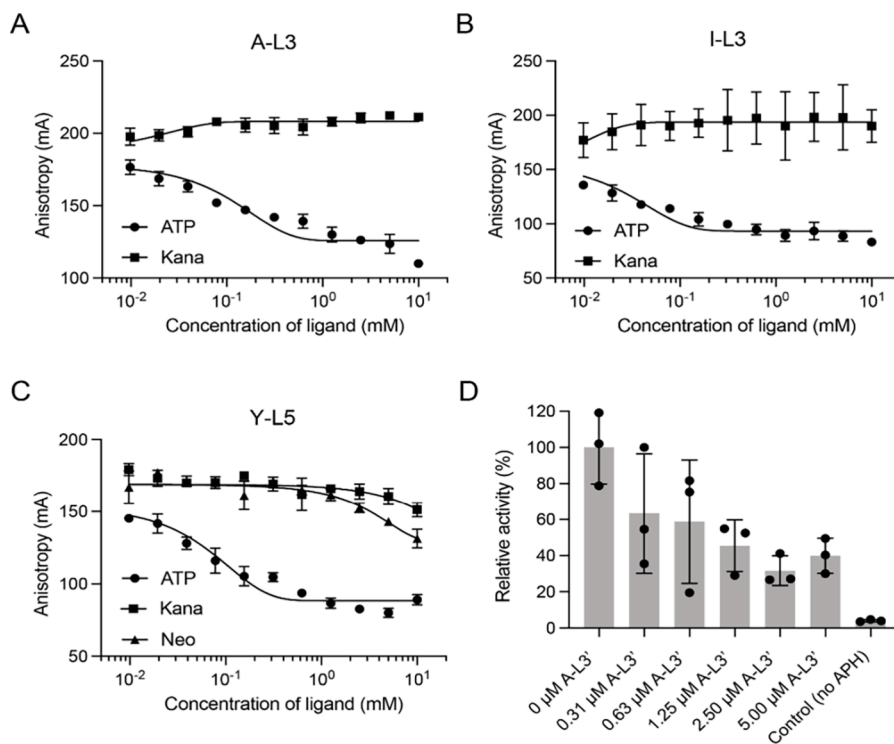
to divalent metal-free conditions. Specifically, K_d values in Mg^{2+}-containing buffer were 0.26 ± 0.02 μM (A-L2), 0.58 ± 0.06 μM (C-L4), and 63 ± 6 nM (I-L3), whereas values in metal-free buffer increased to 0.74 ± 0.07, 1.59 ± 0.25, and 0.42 ± 0.04 μM, respectively. Moderate K_d values were

Figure 6. Identification of binding sites and inhibitory effects of candidate cyclic peptides targeting APH. (A−C) Competitive fluorescence polarization assays showing the effect of varying concentrations of ATP or antibiotics on the binding of cyclic peptides A-L3 (A), I-L3 (B), and Y-L5 (C) to APH. (D) Relative activity of APH measured in the presence of 0−5.0 μM cyclic peptide A-L3′ (without FAM group at C-terminus). The inhibitory activity of peptide I-L3′ is shown in Figure S6. Data are presented as the mean ± standard deviation from three independent measurements.

potent cyclic peptide inhibitors. Conversely, any metal ions that are not present under physiological conditions should be omitted during selection to avoid enriching peptides whose binding depends on non-physiological cations and that would therefore fail to bind *in vivo*.

Binding Site and Inhibition Analysis of Cyclic Peptides. The active sites of APH are ATP-binding site and antibiotic-binding site.[32] To inculcate the candidate cyclic peptide binding site in APH, a competitive fluorescence polarization assay was performed by including ATP or kanamycin into the binding assay. For two candidate cyclic peptides, A-L3 and I-L3, which contain the CXW(P/L)LC motif, Kanamycin showed no effect on the binding reaction, while 0.04−0.16 mM of ATP could affect its binding (Figure 6A,B). In contrast, for Y-L5, which contains the CP(W/F)YC motif, kanamycin and neomycin could partially compete with the Y-L5 binding, while ATP could impede Y-L5 access to the binding site more potently (Figure 6C). The results indicating that all candidate cyclic peptides containing conserved motif CXW(P/L)LC or CP(W/F)YC primarily bind at the ATP-binding site of APH.

To evaluate the inhibitory effect of candidate cyclic peptides, APH activity was measured in the presence of varying concentrations of A-L3′ (A-L3 without a FAM group at C-terminus), with a blank assay consisting of the sample without APH. It was observed that the addition of A-L3′ (0.31−5.00 μM) resulted in a decrease in APH activity compared to the control without A-L3′. At 0.31 μM A-L3′, the relative activity of APH decreased to ~60%, and at 5.00 μM A-L3′, it dropped to ~40% (Figure 6D). These results indicate that the candidate cyclic peptide A-L3′ effectively inhibits APH activity *in vitro*.

To date, the reported APH inhibitors exhibit distinct binding sites and modes. By fusing adenosine and neamine (an aminoglycoside antibiotic) into one compound, bisubstrate analogue inhibitors occupy both of the enzyme's substrate-binding pockets at once.[33] By contrast, adapted from pyrazolopyrimidine inhibitors of ePKs,[37,38] pyrazolopyrimidine derivatives impair APH activity *in vitro* by engaging the NTP-binding site in a conformation that differs from how they bind to ePKs.[32] In the present study, our cyclic peptides also target the ATP-binding cleft of APH (Figure 6A−C), and their broader interaction surface may offer superior selectivity over pyrazolopyrimidine derivatives to better discriminate APH from structurally similar ePKs.

CONCLUSIONS

Using inhibitors of antibiotic-resistant enzymes as adjuvants is a reasonable strategy in response to the antibiotic resistance challenge. However, there are no inhibitors available for aminoglycoside resistance enzymes in clinical use. In this study, we choose APH, which catalyzes aminoglycoside phosphorylation, as a target to fishing candidate inhibitors of cyclic peptides using phage display-based selection.

Our study establishes cyclic peptides as a promising class of inhibitors targeting the ATP-binding cleft of APH, offering a novel strategy to combat aminoglycoside resistance. Through phage display screening of an ultradiverse cyclic peptide library (10^{11} variants), we identified two conserved motifs, CXW(P/L)LC and CP(W/F)YC, which confer nanomolar binding affinities and ATP-competitive inhibition. Mg^{2+} and Ca^{2+} significantly improved peptide−APH interactions (up to a 6.7-fold affinity increase), likely by stabilizing structural conformations critical for target engagement.

In summary, the availability of cyclic peptide inhibitors in our study provides insight into the further development of effective and potent inhibitors for the treatment of AGA-resistant bacteria with APH in clinical use. Future efforts will focus on structural optimization (e.g., through reduced molecular weight and hydrogen-bond donors to improve permeability), followed by *in vivo* validation of optimized leads. Co-crystallization studies of peptide-APH complexes are essential to elucidate binding modes and guide the rational design of cyclic peptides. Additionally, extending this platform to other AMEs (i.e., AACs and ANTs) could broaden its impact on multidrug resistance.

MATERIALS AND METHODS

Preparation of Phage-Displayed Peptide Library. For each sublibrary, 1 mL of library glycerol stock was inoculated into 0.25 L of 2YT medium with 10 μg/mL tetracycline. Then, the mixture was incubated overnight at 30 °C while being shaken at 200 rpm. After centrifugation at 8000 rpm for 20 min to collect the supernatant, 20% (v/v) of ice-cold buffer N (20% (w/v) polyethylene glycol 6000 and 2.5 M NaCl) was added. After incubation on ice for 30 min, the phage was harvested through centrifugation at 6500 rpm for 45 min at 4 °C. The phage pellet was dissolved in 40 mL degassed buffer R (20 mM NH_4HCO_3 and 5 mM EDTA, pH 8.0) and centrifuged again at 6500 rpm for 5 min to remove residual bacterial cells.

The peptides displayed on phages were reduced with 1 mM TCEP at 20 °C for 30 min. Phage was precipitated by adding 10 mL of ice-cold buffer N, followed by centrifugation at 4500 rpm and 4 °C for 15 min. The retrieved phage pellet was then resuspended in 6 mL of degassed buffer R, and the obtained phage solutions were equally divided into eight 4.5 mL aliquots. For each aliquot, 0.5 mL of 200 μM chemical linker was added and the mixture incubated at 30 °C for 1 h. Besides seven chemical linkers, the last aliquot was also incubated at 30 °C for 1 h without linker and used as a control in the following selections. The cyclized peptide library was harvested using phage precipitation, and then resuspended in 5 mL of buffer W2 (10 mM Tris−Cl, 150 mM NaCl, 10 mM $MgCl_2$, 1 mM $CaCl_2$, 1% (w/v) BSA, and 0.1% (v/v) Tween 20, pH 7.4), for the round 3 selection, we took 50 μL of the solution for each as initial phage samples. Then, the phage samples were blocked for 30 min at room temperature (RT) on a rotating wheel (10 rpm).

Phage Selection against APH. To immobilize the biotinylated APH for panning, 160 μL of magnetic beads was washed twice by 1 mL of buffer W1 (10 mM Tris−Cl, 150 mM NaCl, 10 mM $MgCl_2$, and 1 mM $CaCl_2$, pH 7.4) and resuspended in 160 μL of buffer W1. Then, 4 μg of APH-Biotin was added and mixed up, and the reaction was performed for 30 min at RT on a rotating wheel (10 rpm). Magnetic beads were collected and washed twice by 1 mL of buffer W1, then the beads were resuspended in 400 μL of buffer W2 and blocked for 30 min at RT on a rotating wheel (10 rpm).

Two types of beads, streptavidin and neutravidin beads, were used alternatively in the three rounds of phage selection to disfavor enrichment of streptavidin- or neutravidin-specific peptides. Neutravidin beads were prepared by reacting 6 mg of neutravidin (Pierce) with 10 mL of tosyl-activated magnetic beads (Dynal, M-280 from Invitrogen) according to the supplier's instructions. For the first and the third rounds of selection, 4 and 0.4 μg of APH-Biotin were immobilized on 160 and 80 μL of streptavidin beads, respectively. For the second round, 2 μg of APH-Biotin was immobilized on 180 μL of neutravidin beads.

The 50 μL blocked beads were mixed with the 5 mL blocked phage and incubated for 1 h on a rotating wheel (10 rpm) at RT. Subsequently, the beads were collected and washed with buffer W1 containing 0.1% (v/v) Tween 20 eight times and then rinsed twice with buffer W1. The beads with captured phage were incubated with 5 mL *E. coli* TG1 cells (OD600 = 0.4−0.8) for 30 min at 37 °C, and the cells were collected by centrifugation at 5000 rpm for 5 min, then plated on 2YT plates containing tetracycline (10 μg/mL). The plate

was incubated overnight at 37 °C. The obtained cells were resuspended in 4 mL of 2YT medium containing 10% glycerol and stored at −20 °C as stock. Furthermore, for round 2 and round 3 selection, phages were obtained by inoculation of the glycerol stock from a previous round.

NGS Analysis of Enriched Peptides. The peptide-encoding DNA of phage samples was sequenced on the Illumina next-generation sequencing (NGS) platform. NGS samples were prepared following two rounds of PCR reactions using primers containing barcodes and adapter sequences, respectively.

The peptide library glycerol stock or phage samples of three rounds was used as templates of the first PCR reaction. The phage samples from the selection were heated at 95 °C for 10 min and centrifuged to remove protein contents in the sample and release the ssDNA. The first-round PCR reaction was performed in 50 μL containing 1 μL of glycerol stocks (OD600 ~10) or 2 μL of treated phage sample as template, 5 μL of forward primer (1 μM), 5 μL of reverse primer (1 μM), 25 μL of 2× PCR MasterMix (Cat#NG001, HLingene), and added ddH$_2$O up to 50 μL. The PCR procedure was 95 °C for 5 min, followed by 25 cycles of 30 s at 95 °C, 30 s at 55 °C, and 30 s at 72 °C and a final elongation at 72 °C for 10 min. The product of the first round PCR was confirmed with 2.5% agarose gel.

The second round of PCR was performed in 50 μL containing 2 μL of the first PCR product mixture as template, 1 μL of forward primer S505 (5 μM), 1 μL of reverse primer N704 (5 μM), 25 μL of 2× PCR MasterMix (Cat#NG001, HLingene), and added ddH$_2$O up to 50 μL. To get the sufficient product, a total of 200 μL (50 μL × 4 tubes) of PCR reaction was conducted. The PCR procedure was 95 °C for 5 min, followed by 25 cycles of 30 s at 95 °C, 60 s at 55 °C, and 30 s at 72 °C and a final elongation at 72 °C for 10 min. The product of the second round PCR was confirmed with 2.5% agarose gel and purified by the AxyPrep PCR Clean-up Kit. After concentration detection using Qubit, the purified DNA fragments were sequenced with Illumina Novaseq 2× 150 bp (GENEWIZ Ltd., Suzhou, China). The primer sequences used in this study are listed in Table S2.

NGS Data Analysis. The NGS data were analyzed by MatLab scripts as previously described.[34] First, the reads were separated into several files according to the barcode. Second, low-quality sequences of each file were removed, and the remaining sequences were translated into amino acid sequences of peptides; peptides with lengths beyond 5−14 amino acids were excluded. Third, the mutation errors generated in the abundant peptide sequences during the NGS process were fixed. Finally, the obtained peptide sequences were grouped into families based on sequence similarity, and the abundance of selected peptides was further analyzed using Microsoft Excel.

Affinity Assay Using Fluorescence Polarization. Fluorescent cyclic (or linear, oxidized) peptides were diluted to 100 nM in reaction buffer (50 mM Tris−Cl pH 7.5, 40 mM KCl, and 10 mM MgCl$_2$) with the addition of 0.01% Tween 20. Serial 2-fold dilutions of the target protein APH were performed (totally 11 samples) using the reaction buffer (0.01% Tween 20). A sample of reaction buffer (0.01% Tween 20) was used as a control. The assay was conducted in 384-well black plates, and total volume in each well is 15 μL containing 3 μL of peptide solution (final concentration of 20 nM) and 12 μL of APH dilutions. After 30 min of incubation at RT, anisotropy values were measured using a microplate reader (Spark, TECAN). The dissociation constant (K_d) was determined by nonlinear regression analysis of fluorescence anisotropy (Y) versus the final concentration of APH(x) using eq1. GraphPad Prism 9 software was used for data analysis with the fluorescence anisotropy of the free peptide (Af), the fully bound peptide (Ab), and the total concentration of fluorescent ligand $[L]_T$ = 20 nM.

$$A = A_f + (A_b - A_f)$$
$$\times \left\{ \frac{[L]_T + K_D + [P]_T - \sqrt{([L]_T + K_D + [P]_T)^2 - 4[L]_T[P]_T}}{2[L]_T} \right\} \tag{1}$$

Effect of Divalent Metal Ions, ATP, and Kanamycin on Binding. To test the effect of metal ions on binding, three different buffers were used that contained varied concentrations of divalent metal ions: 50 mM Tris (pH 7.5) and 40 mM KCl, with the addition of (i) 10 mM Mg^{2+}, (ii) 1 mM Ca^{2+}, or (iii) no divalent metal ions. The candidate cyclic peptides and APH protein were dissolved in these three buffers (0.01% Tween 20) at appropriate concentration. Then, the affinity of peptide and APH in three different conditions was detected using the same method as described above.

Competitive fluorescence polarization assay was used to determine the effect of ATP or kanamycin on the binding of candidate cyclic peptides to the APH protein. The assay was conducted in 384-well black plates with a total volume of 15 μL in each well. For each cyclic peptide, 20 nM of fluorescent cyclic peptide was mixed with subsaturation concentration of protein APH (0.2 to 1.6 μM) and 0 to 10 mM of ATP or kanamycin. For three candidate cyclic peptides, A-L3, I-L3, and Y-L5, the subsaturation concentrations of APH used were 1.0, 0.2, and 1.6 μM, respectively. Fluorescence anisotropy was measured the same as described above. The data of anisotropy versus the peptide concentration were fitted to the log(inhibitor) versus response equation using nonlinear regression analysis:

$$Y = A_{min} + \frac{A_{max} - A_{min}}{1 + 10^{(\log|C50-X)p}} \tag{2}$$

wherein Y is the anisotropy, X is the logarithm of peptide concentration, A_{min} is the bottom of the fitted anisotropy curve, A_{max} is the top of the fitted anisotropy curve, IC$_{50}$ is the concentration of peptide that inhibits 50% of target-FAM peptide binding, and p is the Hill coefficient.

Inhibition Assay. The specific activities of APH were determined by measuring the transformation of ATP to ADP by HPLC (Agilent 1260 Infinity II). The assay samples were prepared as follows: 0.2 mM ATP-Na$_2$, 0.2 mM kanamycin, 0.1 μM APH, and 0 to 5.0 μM A-L3′ (or I-L3′) were added in a total volume of 100 μL reaction buffer. The control sample (no APH) contained 0.2 mM ATP-Na$_2$ and 0.2 mM kanamycin. The reactions were carried out at 37 °C for 1 h and terminated by adding 40 μL of chloroform into 20 μL of the sample and vortexing for 1 min. All samples were centrifuged at 12,000 × g for 5 min, and the supernatant was used for HPLC analysis.

Concentrations of ATP and ADP were measured with an HPLC equipped with a Thermo Fisher Betasil C18 column (250 × 4.6 mm, 5 μm). Mobile phase A consisted of 0.02 M KH$_2$PO$_4$ (pH = 6.0), and mobile phase B consisted of 100% methanol. The mobile phase composition was 95% A and 5% B, and the flow rate was set to 1 mL/min. The column was maintained at RT. Detection was performed at the wavelength of 254 nm.

■ ASSOCIATED CONTENT

ⓈI Supporting Information

The Supporting Information is available free of charge at https://pubs.acs.org/doi/10.1021/acschembio.5c00366.

> Construction of the phage-displayed peptide library, purification of the target protein, and synthesis of peptides; library design, PCR primers, and a list of synthesized peptides; results of library design and quality assessment, protein purification, LC-MS characterization of peptides, and assays of peptide affinity and inhibitory activity (PDF)

■ AUTHOR INFORMATION

Corresponding Author

Xu-Dong Kong − *State Key Laboratory of Microbial Metabolism, School of Life Sciences & Biotechnology, and Zhangjiang Institute for Advanced Study, Shanghai Jiao Tong University, Shanghai 200240, China;* ⓞ orcid.org/0000-0003-3216-7545; Email: xudong.kong@sjtu.edu.cn

Authors

Qiannan Guo − *State Key Laboratory of Microbial Metabolism, School of Life Sciences & Biotechnology, and Zhangjiang Institute for Advanced Study, Shanghai Jiao Tong University, Shanghai 200240, China*

Hui Zeng − *State Key Laboratory of Microbial Metabolism, School of Life Sciences & Biotechnology, and Zhangjiang Institute for Advanced Study, Shanghai Jiao Tong University, Shanghai 200240, China*

Complete contact information is available at:
https://pubs.acs.org/10.1021/acschembio.5c00366

Author Contributions

Q.N.G. and X.D.K. designed research; Q.N.G. performed research; Q.N.G., H.Z., and X.D.K. wrote the paper.

Notes

The authors declare no competing financial interest.

■ REFERENCES

(1) Salam, M. A.; Al-Amin, M. Y.; Salam, M. T.; Pawar, J. S.; Akhter, N.; Rabaan, A. A.; Alqumber, M. A. A. Antimicrobial resistance: a growing serious threat for global public health. *Healthcare.* **2023**, *11* (13), 1946.

(2) Darby, E. M.; Trampari, E.; Siasat, P.; Gaya, M. S.; Alav, I.; Webber, M. A.; Blair, J. M. A. Molecular mechanisms of antibiotic resistance revisited. *Nat. Rev. Microbiol.* **2023**, *21* (5), 280−295.

(3) Douafer, H.; Andrieu, V.; Phanstiel, O. T.; Brunel, J. M. Antibiotic adjuvants: make antibiotics great again! *J. Med. Chem.* **2019**, *62* (19), 8665−8681.

(4) Costa, B. O.; Cardoso, M. H.; Franco, O. L. Development of peptides that inhibit aminoglycoside-modifying enzymes and *β*-lactamases for control of resistant bacteria. *Curr. Protein Pept. Sci.* **2020**, *21* (10), 1011−1026.

(5) Katsarou, A.; Stathopoulos, P.; Tzvetanova, I. D.; Asimotou, C. M.; Falagas, M. E. *β*-Lactam/*β*-lactamase inhibitor combination antibiotics under development. *Pathogens.* **2025**, *14* (2), 168.

(6) Becker, B.; Cooper, M. A. Aminoglycoside antibiotics in the 21st century. *ACS Chem. Biol.* **2013**, *8* (1), 105−115.

(7) Shandrick, S.; Zhao, Q.; Han, Q.; Ayida, B. K.; Takahashi, M.; Winters, G. C.; Simonsen, K. B.; Vourloumis, D.; Hermann, T. Monitoring molecular recognition of the ribosomal decoding site. *Angew. Chem., Int. Ed.* **2004**, *43* (24), 3177−3182.

(8) Puglisi, J. D.; Blanchard, S. C.; Dahlquist, K. D.; Eason, R. G.; Fourmy, D.; Lynch, S. R.; Recht, M. I.; Yoshizawa, S. Aminoglycoside antibiotics and decoding.*The Ribosome: Structure, Function, Antibiotics, and Cellular Interactions*; Garrett, R. A.; Douthwate, S. R.; Matheson, A. T., Eds.;.American Society for Microbiology Press, 2000; 419−429.

(9) Ramirez, M. S.; Tolmasky, M. E. Aminoglycoside modifying enzymes. *Drug Resist. Updat.* **2010**, *13* (6), 151−171.

(10) Siregar, J. J.; Miroshnikov, K.; Mobashery, S. Purification, characterization, and investigation of the mechanism of aminoglycoside 3′-phosphotransferase type Ia. *Biochemistry.* **1995**, *34* (39), 12681−12688.

(11) Oka, A.; Sugisaki, H.; Takanami, M. Nucleotide sequence of the kanamycin resistance transposon Tn903. *J. Mol. Biol.* **1981**, *147* (2), 217−226.

(12) Vakulenko, S. B.; Mobashery, S. Versatility of aminoglycosides and prospects for their future. *Clin. Microbiol. Rev.* **2003**, *16* (3), 430−450.

(13) Shaw, K. J.; Rather, P. N.; Hare, R. S.; Miller, G. H. Molecular genetics of aminoglycoside resistance genes and familial relationships of the aminoglycoside-modifying enzymes. *Microbiol. Rev.* **1993**, *57* (1), 138−163.

(14) Bacot-Davis, V. R.; Bassenden, A. V.; Berghuis, A. M. Drug-target networks in aminoglycoside resistance: hierarchy of priority in structural drug design. *MedChemComm.* **2016**, *7*, 103−113.

(15) Ji, X.; Nielsen, A. L.; Heinis, C. Cyclic peptides for drug development. *Angew. Chem., Int. Ed.* **2024**, *63* (3), No. e202308251.

(16) Vinogradov, A. A.; Yin, Y.; Suga, H. Macrocyclic peptides as drug candidates: recent progress and remaining challenges. *J. Am. Chem. Soc.* **2019**, *141* (10), 4167−4181.

(17) Smith, G. P. Filamentous fusion phage: novel expression vectors that display cloned antigens on the virion surface. *Science.* **1985**, *228* (4705), 1315−1317.

(18) Smith, G. P. Phage display: simple evolution in a petri dish (Nobel lecture). *Angew. Chem., Int. Ed.* **2019**, *58* (41), 14428−14437.

(19) Bain, B.; Brazil, M. Adalimumab. *Nat. Rev. Drug Discovery* **2003**, *2* (9), 693−694.

(20) Heinis, C.; Rutherford, T.; Freund, S.; Winter, G. Phage-encoded combinatorial chemical libraries based on bicyclic peptides. *Nat. Chem. Biol.* **2009**, *5* (7), 502−507.

(21) Zuraw, B.; Yasothan, U.; Kirkpatrick, P. Ecallantide. *Nat. Rev. Drug Discovery* **2010**, *9* (3), 189−190.

(22) Bennett, G.; Harrison, H.; Campbell, S.; Teufel, D.; Langford, G.; Watt, A.; Bonny, C. Development of BT1718, a Bicycle Drug Conjugate® (BDC) targeting MT1-MMP for treatment of solid tumours. *Eur. J. Cancer.* **2016**, *69*, S21.

(23) Chen, S. Y.; Morales-Sanfrutos, J.; Angelini, A.; Cutting, B.; Heinis, C. Structurally diverse cyclisation linkers impose different backbone conformations in bicyclic peptides. *ChemBioChem.* **2012**, *13* (7), 1032−1038.

(24) Chen, S. Y.; Bertoldo, D.; Angelini, A.; Pojer, F.; Heinis, C. Peptide ligands stabilized by small molecules. *Angew. Chem., Int. Ed. Engl.* **2014**, *53* (6), 1602−1606.

(25) He, R. N.; Zhang, M. J.; Dai, B.; Kong, X. D. Selection of peptide-bismuth bicycles using phage display. *ACS Chem. Biol.* **2024**, *19* (5), 1040−1044.

(26) Ullrich, S.; Somathilake, U.; Shang, M.; Nitsche, C. Phage-encoded bismuth bicycles enable instant access to targeted bioactive peptides. *Commun. Chem.* **2024**, *7* (1), 143.

(27) Kale, S. S.; Villequey, C.; Kong, X. D.; Zorzi, A.; Deyle, K.; Heinis, C. Cyclization of peptides with two chemical bridges affords large scaffold diversities. *Nat. Chem.* **2018**, *10* (7), 715−723.

(28) Kong, X. D.; Moriya, J.; Carle, V.; Pojer, F.; Abriata, L. A.; Deyle, K.; Heinis, C. De novo development of proteolytically resistant therapeutic peptides for oral administration. *Nat. Biomed. Eng.* **2020**, *4* (5), 560−571.

(29) Owens, A. E.; Iannuzzelli, J. A.; Gu, Y.; Fasan, R. MOrPH-PhD: An integrated phage display platform for the discovery of functional genetically encoded peptide macrocycles. *ACS Cent. Sci.* **2020**, *6* (3), 368−381.

(30) Bechtler, C.; Lamers, C. Macrocyclization strategies for cyclic peptides and peptidomimetics. *RSC Med. Chem.* **2021**, *12* (8), 1325−1351.

(31) Hampton, J. T.; Liu, W. R. Diversification of phage-displayed peptide libraries with noncanonical amino acid mutagenesis and chemical modification. *Chem. Rev.* **2024**, *124* (9), 6051−6077.

(32) Stogios, P. J.; Spanogiannopoulos, P.; Evdokimova, E.; Egorova, O.; Shakya, T.; Todorovic, N.; Capretta, A.; Wright, G. D.; Savchenko, A. Structure-guided optimization of protein kinase inhibitors reverses aminoglycoside antibiotic resistance. *Biochem. J.* **2013**, *454* (2), 191−200.

(33) Liu, M.; Haddad, J.; Azucena, E.; Kotra, L. P.; Kirzhner, M.; Mobashery, S. Tethered bisubstrate derivatives as probes for mechanism and as inhibitors of aminoglycoside 3′-phosphotransferases. *J. Org. Chem.* **2000**, *65* (22), 7422−7431.

(34) Rentero Rebollo, I.; Sabisz, M.; Baeriswyl, V.; Heinis, C. Identification of target-binding peptide motifs by high-throughput

sequencing of phage-selected peptides. *Nucleic Acids Res.* **2014**, *42* (22), No. e169.

(35) Boehr, D. D.; Draker, K. A.; Koteva, K.; Bains, M.; Hancock, R. E.; Wright, G. D. Broad-spectrum peptide inhibitors of aminoglycoside antibiotic resistance enzymes. *Chem. Biol.* **2003**, *10* (2), 189−196.

(36) Hon, W. C.; McKay, G. A.; Thompson, P. R.; Sweet, R. M.; Yang, D. S.; Wright, G. D.; Berghuis, A. M. Structure of an enzyme required for aminoglycoside antibiotic resistance reveals homology to eukaryotic protein kinases. *Cell.* **1997**, *89* (6), 887−895.

(37) Apsel, B.; Blair, J. A.; Gonzalez, B.; Nazif, T. M.; Feldman, M. E.; Aizenstein, B.; Hoffman, R.; Williams, R. L.; Shokat, K. M.; Knight, Z. A. Targeted polypharmacology: discovery of dual inhibitors of tyrosine and phosphoinositide kinases. *Nat. Chem. Biol.* **2008**, *4* (11), 691−699.

(38) Knowles, P. P.; Murray-Rust, J.; Kjaer, S.; Scott, R. P.; Hanrahan, S.; Santoro, M.; Ibanez, C. F.; McDonald, N. Q. Structure and chemical inhibition of the RET tyrosine kinase domain. *J. Biol. Chem.* **2006**, *281* (44), 33577−33587.